ELSEVIER

Thermochimica Acta 273 (1996) 145–156

thermochimica acta

Properties of the products of basic aluminium-ammonium sulphate decomposition in hydrogen atmosphere and of the aluminium oxides obtained by their calcination

Barbara Pacewska, Tadeusz Żmijewski, Maria Mioduska

Institute of Chemistry, Płock Branch of Warsaw University of Technology, Łukasiewicza 17, 09-400 Płock, Poland

Received 31 March 1995; accepted 27 May 1995

Abstract

The physicochemical properties of aluminium oxide obtained by decomposition of basic aluminium-ammonium sulphate in a hydrogen atmosphere at 700°C were studied. The effect of calcination conditions on the changes in phase composition and porous structure of the aluminium oxides formed was determined. The increase in calcination temperature was accompanied by a decrease in the specific surface of the products, as well as in the volume and surface of the pores having $d/2$ within 30–15 Å. At the same time the volume and the surface of pores having $d/2$ within 100–60 Å increased with increasing temperature.

Keywords: Active alumina; Reduction calcination; Synthetic alunite

1. Introduction

Former studies on the steps and kinetics of the decomposition of basic aluminium-ammonium sulphate in a hydrogen atmosphere [1, 2] have shown that a low-temperature aluminium oxide can be obtained by performing the process for 2 h at 700°C or a higher temperature. One aim of this work was to study the physicochemical properties of aluminium oxide obtained by decomposition of basic aluminium-ammonium sulphate in a hydrogen atmosphere at 700°C.

The preparation of low-temperature modifications of aluminium oxide from potassium alunite yields mixtures of γ-Al_2O_3 and K_2SO_4 [3, 4]. When the potassium compounds contained in the mixture are leached out, the resulting hydrous aluminium oxide has a much higher specific surface and pore volume than non-leached samples

SSDI 0040-6031(95)02547-2

[5,6]. In order to compare the properties of aluminium oxides obtained from potassium and ammonium alunites, we studied the rehydrated products of basic aluminium-ammonium sulphate decomposition in a hydrogen atmosphere.

The second aim of this work was to study the properties of rehydrated aluminium oxides obtained from ammonium alunite and their calcination products in air at different temperatures with particular consideration to changes in the phase composition and in porous structure.

2. Experimental

Physicochemical properties were studied for the following materials:

(a) The product of the calcination for 2 h at 700°C of basic aluminium-ammonium in a hydrogen atmosphere (sample A/700/H_2);
(b) The product of the hydrothermal treatment of the A/700/H_2 sample (sample A/700/H_2/W);
(c) The products of the calcination of sample A/700/H_2/W in air for 2 h at 400, 600, 800 and 1000°C, denoted A/700/H_2/W/400, A/700/H_2/W/600, A/700/H_2/W/800 and A/700/H_2/W/1000, respectively.

The samples were heated in air atmosphere in a Derivatograph C produced by MOM, Budapest, reaching the required temperature with a heating rate of 10 K min^{-1}.

The rehydration of the decomposition products was performed by mixing the sample with demineralized water (100 ml water per 1 g of sample material) and heating, under continuous stirring, for 30 min at 70°C. The heating was repeated twice, and the product was dried for 3 h at 105°C. The sample symbol was supplemented by W, e.g. A/700/H_2/W. The samples were subjected to the following determinations:

(a) Determination of phase composition by X-ray diffraction. The diffraction patterns were recorded in an HZG-4C diffractometer produced by Carl Zeiss, Jena, using CoKα radiation;
(b) The specific surface S_{BET} and the pore surface and volume distribution as a function of pore radius, based on low-temperature isotherms of nitrogen sorption;
(c) Infrared absorption spectra by means of a Specord 75 IR spectrophotometer, using KBr disks;
(d) Granulometric composition by means of the gravitational method using a Shimadzu (Japan) centrifuge;
(e) Morphology of the samples with the use of a TESLA BS-300 scanning electron microscope.

3. Results and discussion

The results obtained are presented in Figs. 1–11 and in Tables 1 and 2. Analysis of the X-ray diffraction pattern of the sample A/700/H_2 (Fig. 1) and the results of kinetic

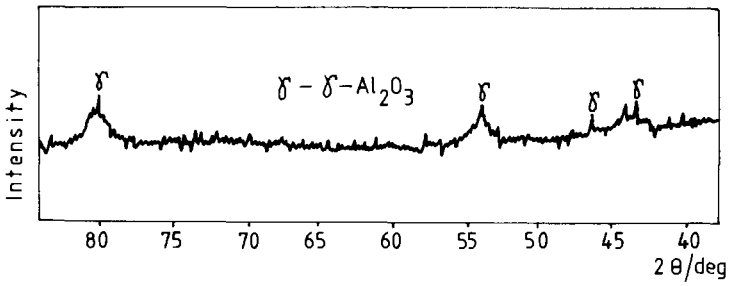

Fig. 1. X-ray diffraction pattern of A/700/H_2 sample.

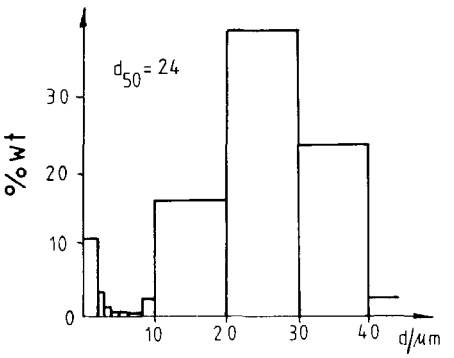

Fig. 2. Granulometric composition of A/700/H_2 sample.

studies [2] showed that the product of basic aluminium-ammonium sulphate decomposition under such conditions is γ-Al_2O_3 of specific surface 109 $m^2 g^{-1}$ and granulometric composition shown in Fig. 2. The material obtained on hydrothermal treatment of the sample contained pseudo-boehmite, detected by X-ray diffraction, accompanying the γ-Al_2O_3 (Fig. 3). The presence of pseudo-boehmite was also confirmed by the results of infrared absorption and thermogravimetric analyses (Figs. 4 and 5). The infrared spectra revealed the presence of absorption bands at wave numbers 1073 and 3100 cm^{-1}, characteristic for pseudo-boehmite. In the DTG curve (Fig. 5) one can observe a peak at 430°C, corresponding to the decomposition of pseudo-boehmite.

Heating the A/700/H_2/W sample at 400°C in air results in the decomposition of pseudo-boehmite, evidenced by the disappearance of the absorption bands at 1073 and 3100 cm^{-1} (Fig. 4). The observed band at 400–1000 cm^{-1} is due to the presence of γ-Al_2O_3. The X-ray diffraction pattern contains reflections due solely to γ-Al_2O_3 (Fig. 3).

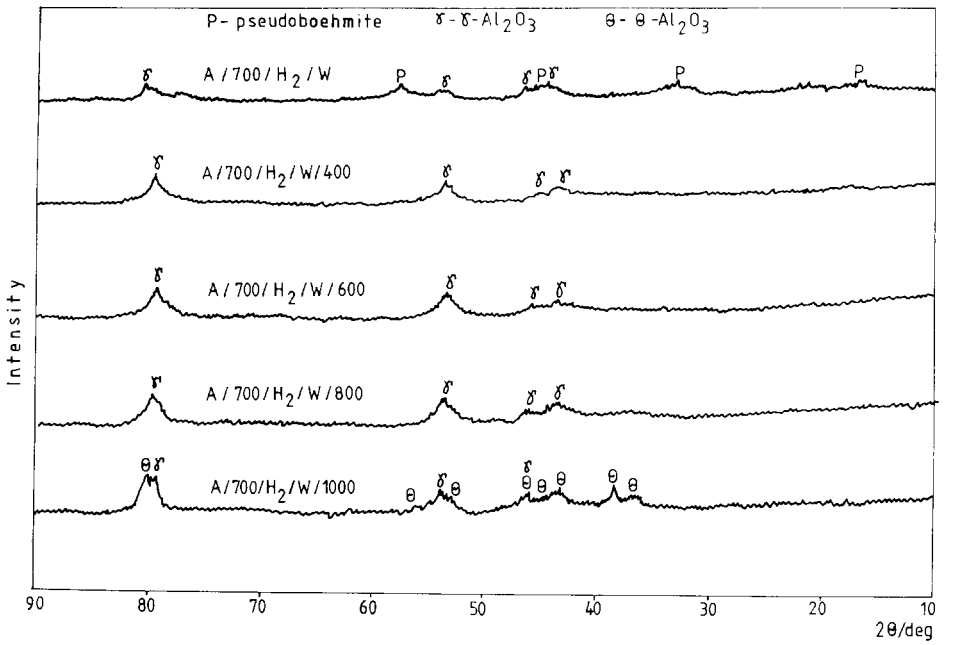

Fig. 3. X-ray diffraction patterns of aluminium oxides obtained from basic aluminium-ammonium sulphate and calcined in air at various temperatures.

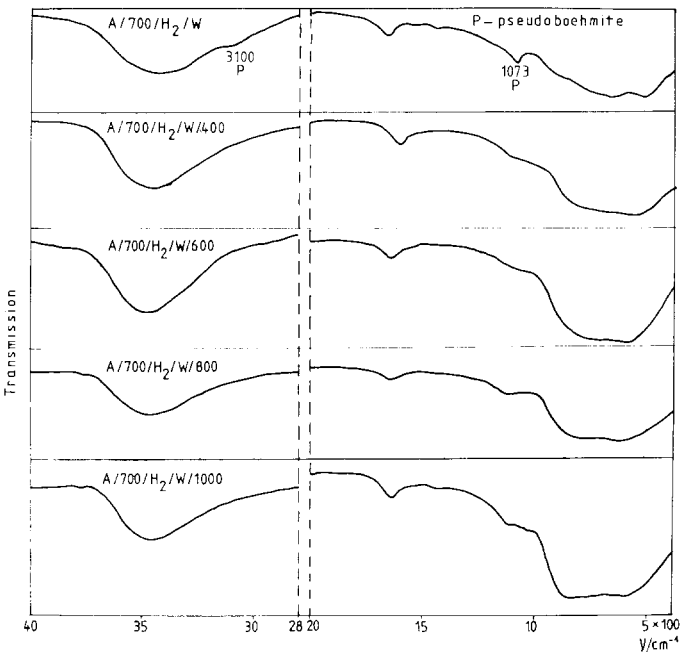

Fig. 4. Infrared spectra of aluminium oxides obtained from basic aluminium-ammonium sulphate.

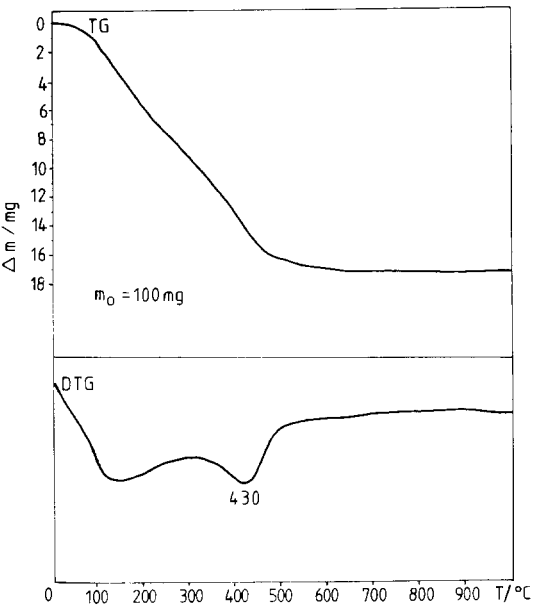

Fig. 5. Thermogravimetric curves of A/700/H_2/W sample.

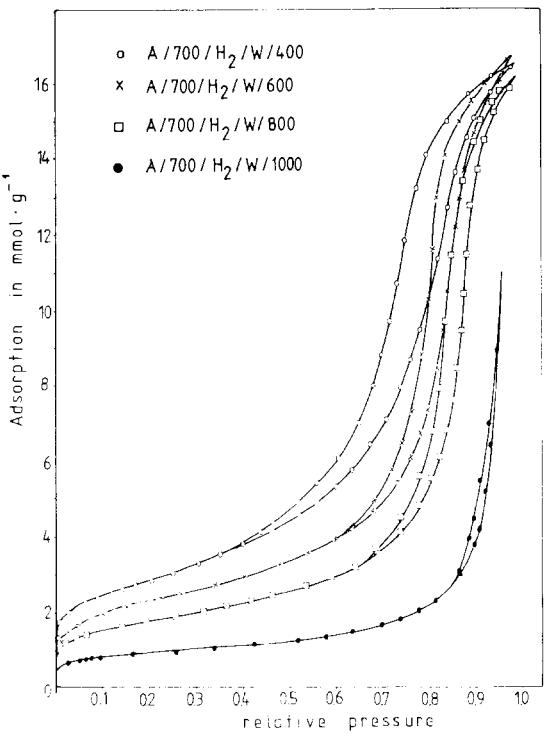

Fig. 6. Nitrogen adsorption and desorption isotherms of calcination products of aluminium oxide obtained by decomposition of basic aluminium-ammonium sulphate.

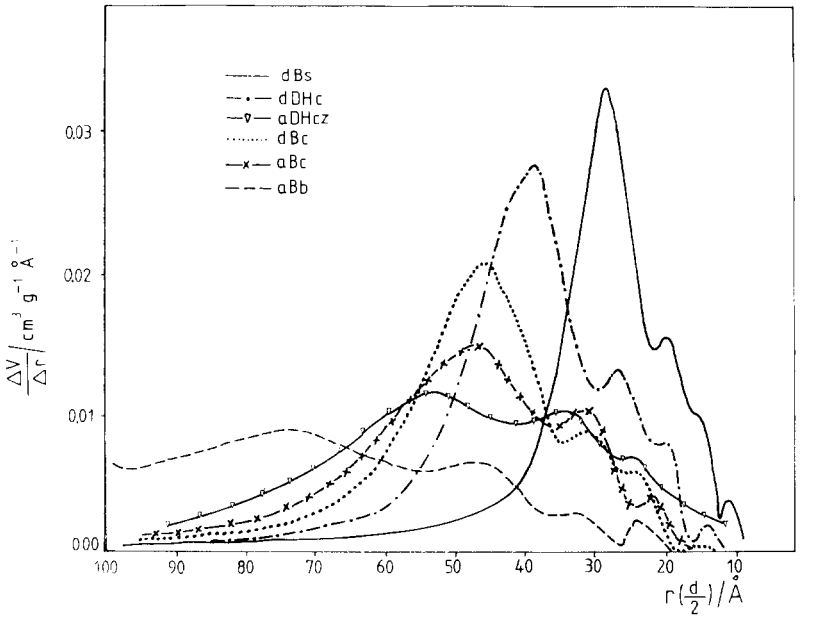

Fig. 7. Distribution of pore volumes as a function of pore radii in A/700/H_2/400 sample calculated by different methods (explanation of symbols given in the text).

Fig. 8. Scanning electron micrograph of A/700/H_2/W sample.

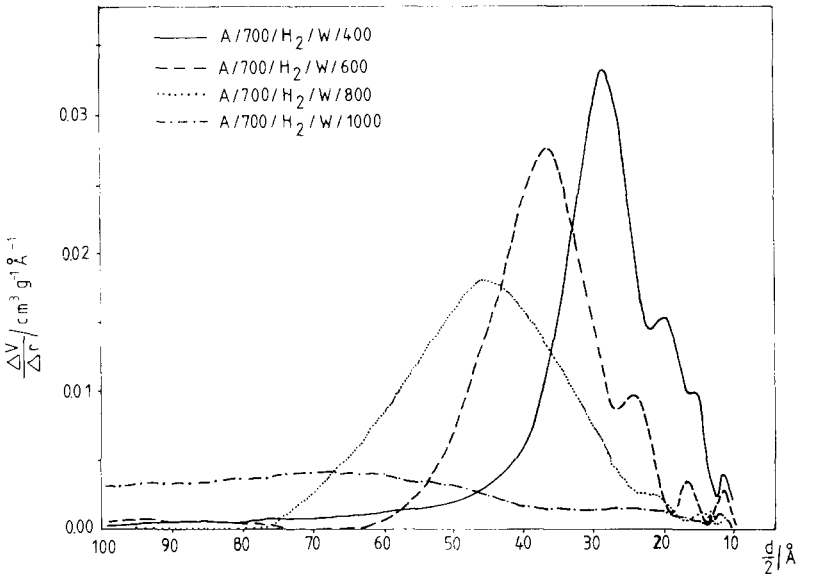

Fig. 9. Distribution of pore volumes of aluminium oxides calculated by the Broekhoff–de Boer method for a model of slot-shaped pores.

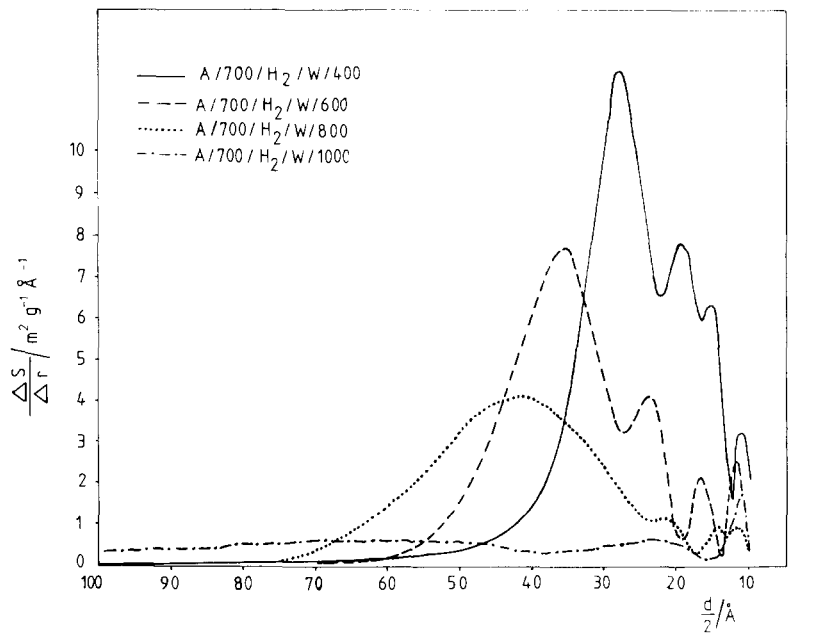

Fig. 10. Distribution of pore surface area of aluminium oxides calculated by the Broekhoff–de Boer method for a model of slot-shaped pores.

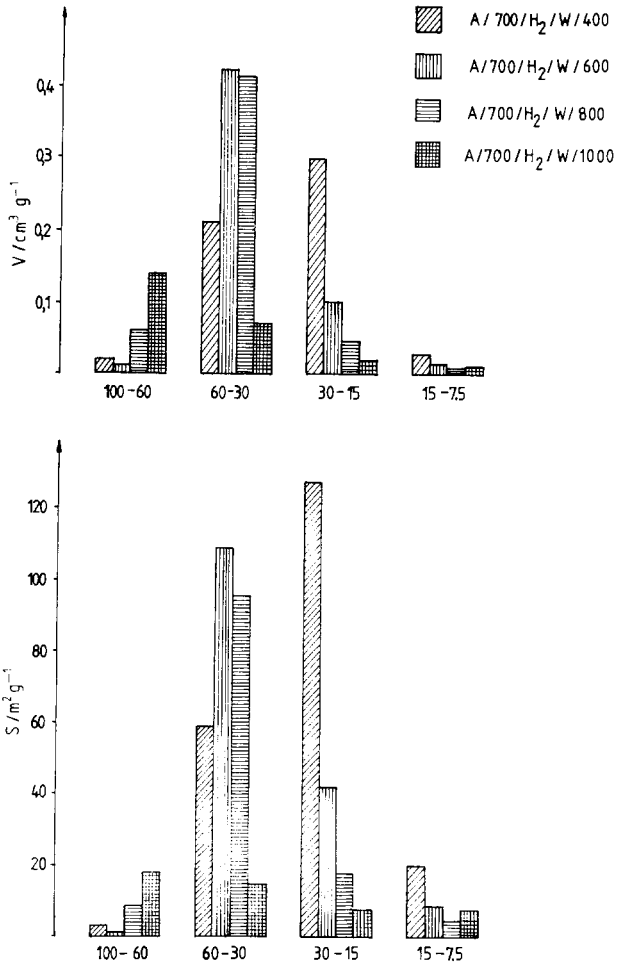

Fig. 11. Distribution of pore volumes and surface area of calcination products of aluminium oxide obtained from basic aluminium-ammonium sulphate.

The specific surface of the A/700/H_2/W/400 sample is about twice that of the sample before the hydrothermal treatment (see the data in Table 1). Calcination of the sample A/700/H_2/W at 600, 800 or 1000°C in an air atmosphere results in further growth of the crystalline structure of the aluminium oxides (Fig. 3). Analysis of the X-ray diffraction patterns showed that calcination at temperatures not exceeding 800°C does not alter the crystallographic form of γ-Al_2O_3, although the presence of small amounts of θ-Al_2O_3 in the A/700/H_2/W/800 sample cannot be excluded. The product of calcination at 1000°C is a mixture of θ- and γ-modifications of Al_2O_3.

The presented course of transformations does not contradict the scheme of pseudoboehmite transformations proposed by Lippens and Steggerda [7]. The observed

Table 1
Pore structure parameters of aluminium oxides obtained from basic aluminium-ammonium sulphate

Parameter	A/700/H_2/W/400	A/700/H_2/W/600	A/700/H_2/W/800	A/700/H_2/W/1000
$S_{BET}/m^2 g^{-1}$	225.4	175.9	135.5	68.2
$S_t/m^2 g^{-1}$	225.0	174.5	130.9	61.7
$V_{mi}/cm^3 g^{-1}$	0.0009	0.0012	0.0028	0.0033
$(\Sigma\Delta S)_{r>10.5}/m^2 g^{-1}$				
aDHcz[a]	282	210	155	69
aBc	245	195	152	60
aBb	242	189	134	58
dDHc	355	246	188	68
dBc	253	186	137	49
dBs	210	161	127	48
$(\Sigma\Delta S)_{r>15}/m^2 g^{-1}$				
aDHcz[a]	266	205	152	55
aBc	240	192	152	53
aBb	236	177	122	54
dDHc	355	246	188	55
dBc	253	185	137	42
dBs	210	161	127	48

[a] Calculation methods have been given in the text.

Key: V_{mi}, volume of micropores as determined by the de Boer's t-method; $(\Sigma\Delta S)_{r>10.5}$, surface area of pores with radii greater than 10.5 Å; $(\Sigma\Delta S)_{r>15}$, surface area of pores with radii greater than 10.5 Å.

changes in crystalline structure and phase composition of the samples are accompanied by modifications in their porous structure. The shape of the nitrogen adsorption isotherms (Fig. 6) points clearly to a dominance of mesopores in the porous structure of the samples.

In order to enable a complex description of the porous structure and selection of the most probable model of pore shapes, a computer program has been developed [8] to permit the calculation of:

- Specific surface by the BET and t–de Boer S_t [9] methods,
- Volume of the micropores by the t–de Boer's method [9],
- Distribution of the pore volume and surface area as a function of their effective radii (or pore half-width in the case of the slot pore model).

The distribution of pore volume and surface area as a function of their radii was calculated from adsorption isotherms by means of the following methods:

- The Broekhoff–de Boer method for a cylindrical model open from both ends (aBc) [10];
- The Dollimore and Heal method for a cylindrical model closed from one end (aDHcz) [11];

Table 2
Distribution of pore volume and surface area calculated by the Broekhoff–de Boer method for a model of slot-shaped pores

	A/700/H_2/W/400	A/700/H_2/W/600	A/700/H_2/W/800	A/700/H_2/W/1000
Volumes of pores in $cm^3 g^{-1}$ with $d/2$ in Å				
100–60	0.0236	0.0110	0.0589	0.1415
60–30	0.2096	0.4222	0.4145	0.0673
30–15	0.2982	0.0998	0.0443	0.0173
15–7.5	0.0254	0.0101	0.0060	0.0083
$\Sigma\Delta V_p$	0.5568	0.5431	0.5237	0.2344
$V_{0.93}$	0.5618	0.5520	0.5340	0.2774
Surface area of pores in $m^2 g^{-1}$ with $d/2$ in Å				
100–60	3.2	1.3	9.1	18.2
60–30	58.6	108.5	94.9	14.5
30–15	127.4	41.7	18.0	7.5
15–7.5	20.4	9.3	5.1	8.0
$\Sigma\Delta S_p$	209.6	160.8	127.1	48.2
S_{BET}	225.4	175.9	135.5	68.2

$d/2$ pore half width; $V_{0.93}$, volume of pores corresponding to N_2 adsorption at a pressure of $p/p_o = 0.93$

- The Broekhoff–de Boer method for the model with bottle-shaped pores (aBb) [12].

The desorption part of the isotherms was treated in terms of the following methods:

- The Broekhoff–de Boer method for a model of cylindrical pores open from both ends (dBc) [13];
- The Dollimore and Heal method for the model of cylindrical pores open from both ends (dDHc) [11];
- The Broekhoff–de Boer method for a model of slot-shaped pores (dBs) [14].

Examples of pore volume distribution for the A/700/H_2/W/400 sample are presented in Fig. 7.

Table 1 comprises the results of calculations by the above methods. Analyses of these results showed that an increase in calcination temperature results in decreased S_{BET} and S_t values of surface area. The good conformity of surface area values found by the BET and t–de Boer's methods, and the negligible volume of the micropores should be noted.

The authors of the above-cited methods for calculation of pore volume and surface area distributions used them for pore sizes exceeding 7.5Å. However, these methods, based on capillary condensation equations, may be applied without restrictions to calculation of the distribution of mesopores, i.e. pores with radii greater than 15 Å. Table 1 presents the results of calculation of the surface area of pores with radii greater

than 10.5 Å and of those greater than 15 Å. The pore surface area calculated for either of these two pore sizes is in most cases higher than the S_{BET}, and only the results derived from the Broekhoff–de Boer method, for the model of slot-shaped pores, give values close to the S_{BET} and S_t values. It may be concluded, therefore, that the model of slot-shaped pores is the most appropriate for description of the porous structure of the materials under study. This conclusion is supported by the results of microscopic observations using scanning electron microscopy (see Fig. 8).

The curves of distribution of pore volume and pore surface area (Figs. 9 and 10) exhibit distinct shifts of maxima toward the larger half-widths as the calcination temperature is raised. By analogy to the description of the effect of calcination temperature on the porous structure of aluminium oxides obtained by reductive decomposition of potassium alunite [6], we have distinguished four groups of pore sizes in the following ranges: 100–60, 60–30, 30–15, and 15–7.5 Å. The changes in pore volumes and surface area within these groups as a function of calcination temperature are given in Table 2 and in the histograms of Fig. 11. It may be seen that increasing the calcination temperature is accompanied by a decrease in the volume and surface area of pores with $d/2$ in the range 30–15 Å, and an increase in the volume and surface area of pores with $d/2$ within 100–60 Å. The increase in calcination temperature of aluminium oxides is apparently accompanied by recrystallization processes, growth of crystallites, and sintering.

4. Conclusions

1. Calcination of basic aluminium-ammonium sulphate at 700°C in hydrogen atmosphere results in the formation of γ-Al_2O_3 of highly developed specific surface. Active alumina can also be obtained by decomposition of basic aluminium-potassium sulphate at 600°C [3] in hydrogen atmosphere, after washing out the potassium compounds.
2. The process of rehydration of the product of calcination of basic aluminium-ammonium sulphate leads to formation of a mixture of γ-Al_2O_3 and pseudo-boehmite, which is characterized by an almost twice as large specific surface area and a highly developed structure of mesopores.
3. The calcination of the rehydration products in air atmosphere at different temperatures within 400–1000°C makes it possible to modify the porous structure and the phase composition of aluminium oxides.
4. Aluminium oxides obtained by calcination of ammonium and potassium alunites in hydrogen atmosphere with subsequent rehydration differ in grain shape and size and in porous structure.

Acknowledgements

The authors would like to express their thanks to Mr. Z. Wenda for carrying out the calculations.

References

[1] B. Pacewska and J. Pysiak, J. Therm. Anal., 37 (1991) 1665.
[2] B. Pacewska and J. Pysiak, J. Therm. Anal., 37 (1991) 1389.
[3] B. Pacewska and J. Pysiak, Thermochim. Acta, 179 (1991) 187.
[4] B. Pacewska, J. Therm. Anal., 36 (1990) 2021.
[5] B. Pacewska, T. Zmijewski and M. Mioduska, J. Therm. Anal., 43 (1995) 103.
[6] T. Zmijewski, B. Pacewska and J. Pysiak, J. Therm. Anal., 43 (1995) 113.
[7] B.C. Lippens and J.J. Steggerda, in B.G. Linsen (Ed.), Physical and Chemical Aspects of Adsorbents and Catalysts, Academic Press, London, 1970, p.171.
[8] Z. Wenda, Master Degree's Thesis, Institute of Chemistry, Plock Branch of Warsaw University of Technology, Plock, 1994.
[9] J.C.P. Broekhoff and B.G. Linsen, in B.G. Linsen (Ed.), Physical and Chemical Aspects of Adsorbents and Catalysts, Academic Press, London, 1970, p.1.
[10] J.C.P.Broekhoff and J.H. de Boer, J. Catal., 9 (1967) 8; 9 (1968) 15.
[11] D. Dollimore and G.R. Heal, J. Colloid Interface Sci., 35 (1970) 508.
[12] J.C.P. Broekhoff and J.H. de Boer, J. Catal., 10 (1968) 153.
[13] J.C.P. Broekhoff and J.H. de Boer, J. Catal., 10 (1968) 368; 377.
[14] J.C.P. Broekhoff and J.H. de Boer, J. Catal.., 10 (1968) 391.